

Cumulative Cyclic Deformation Capacity of Circular Tubular Braces under Local Buckling

Toru Takeuchi, A.M.ASCE¹; and Ryota Matsui²

Abstract: Tubular-section members are commonly used as seismic-resistant braces because they have a higher moment of inertia than open cross sections of equivalent area. However, the cumulative cyclic deformation capacity of tubular sections after buckling is smaller than that of open sections, such as H-shaped sections, because fracture is initiated by local buckling of circular tubular sections. To evaluate the seismic performance of such diagonal braces, it is essential to predict the cumulative cyclic deformation capacity of these braces before any fracturing. In this study, the cumulative cyclic deformation capacity of circular tube braces under local buckling was assessed by performing cyclic loading tests for a range of slenderness and diameter-to-thickness ratios. The mechanism of strain concentration in the tubular braces was studied in various types of analysis, and a method is proposed for assessing the cumulative deformation capacity before fracture based on the entire axial deformation of the braces. DOI: 10.1061/(ASCE)ST.1943-541X.0000380. © 2011 American Society of Civil Engineers.

CE Database subject headings: Bracing; Buckling; Cyclic loads; Deformation.

Author keywords: Circular tubular brace; Local buckling; Cyclic loading; Cumulative deformation.

Introduction

Closed-section structural steel elements, such as circular tubes, are commonly used in seismic-resistant systems as diagonal braces. When exposed to a seismic force that exceeds their buckling force, these tubular sections sustain cyclic loading after buckling. Various hysteresis curve models of such braces have been proposed (Igarashi et al. 1972; Prathuangsit et al. 1978; Jain et al. 1978; Popov et al. 1979; Shibata et al. 1982; Nonaka 1983, 1984a, b), and are commonly used in time-history response analysis of braced structures, including their postbuckling behavior. However, experimental studies conducted by Jain et al. (1980), Tremblay (2002), Elchalakani et al. (2003), and Ookouchi et al. (2005) report that closed-section braces are known to buckle locally at large deformations, which results in fracture at several cycles when axial strain amplitude exceeds several percent. Therefore, when such closed-section members undergo a large earthquake, they are likely to fracture; however, such fractures are difficult to assess in regular macroelement modeling. The results of these studies also indicate that the fatigue life of closed-section members depends on their slenderness and diameter-to-thickness ratios, and that local buckling leads to a decrease in their cumulative deformation capacity. Tang et al. (1989) proposed formulas to evaluate cumulative deformation capacity on the basis of diameter-to-thickness and slenderness ratios. However, effects of deformation amplitude on the cumulative deformation capacity were not considered. Kanvinde and Deierlein (2007) proposed the use of a micromechanics-based

fracture model of large-scale structural components based on experience with detailed finite-element method (FEM) analyses. However, such analyses are time-consuming and, hence, impractical for analyzing multistory structures comprising large numbers of braces.

In the present study, circular tube braces with various slenderness and diameter-to-thickness ratios were subjected to cyclic loading experiments until the instant of fracture. The experimental results were used to develop the relationship between cumulative deformation capacity and these parameters. The buckling hysteresis in tubular sections that exhibited substantial deformation was studied by FEM analysis, and the fracture mechanism of these sections was investigated by examining the local strain in the buckling zone which leads the fatigue fracture. Then, a strain concentration ratio index was introduced to estimate the local strain in the buckling zone using simplified models, and a method was proposed for easy evaluation of the cumulative deformation capacity before fracture without the use of FEM analysis.

Cyclic Loading Tests on Circular Tube Braces

Cyclic loading tests were performed on 10 circular tube brace specimens of different slenderness ratios λ and diameter-to-thickness ratios D/t . Fig. 1(a) shows the test setup for the quasistatic test. Specimens have pin ends; one pin was attached to the reaction frame, and the other to the sliding plate in conjunction with an actuator. L denotes the distance between the pin ends. Longitudinal deformation δ was measured by extensometers placed between both ends of the braces (J_1, J_2). The axial force on the specimen P was calculated by the horizontal force of the sliding plate P_H measured from the load cell installed in the actuator as in Eq. (1), and the normalized axial deformation ε_n and the normalized force σ_n used as indexes for postbuckling phases are defined as in Eq. (2):

$$P = \frac{P_H}{\cos \xi} \quad (1)$$

¹Professor, Dept. of Architecture and Building Engineering, Tokyo Institute of Technology, M1-29, 2-12-1 O-okayama, Meguro-ku, Tokyo, 152-8552 (corresponding author). E-mail: ttoru@arch.titech.ac.jp

²Graduate Student, Dept. of Architecture and Building Engineering, Tokyo Institute of Technology, M1-29, 2-12-1 O-okayama, Meguro-ku, Tokyo, 152-8552.

Note. This manuscript was submitted on October 28, 2009; approved on January 3, 2011; published online on January 5, 2011. Discussion period open until April 1, 2012; separate discussions must be submitted for individual papers. This paper is part of the *Journal of Structural Engineering*, Vol. 137, No. 11, November 1, 2011. ©ASCE, ISSN 0733-9445/2011/11-1311-1318/\$25.00.

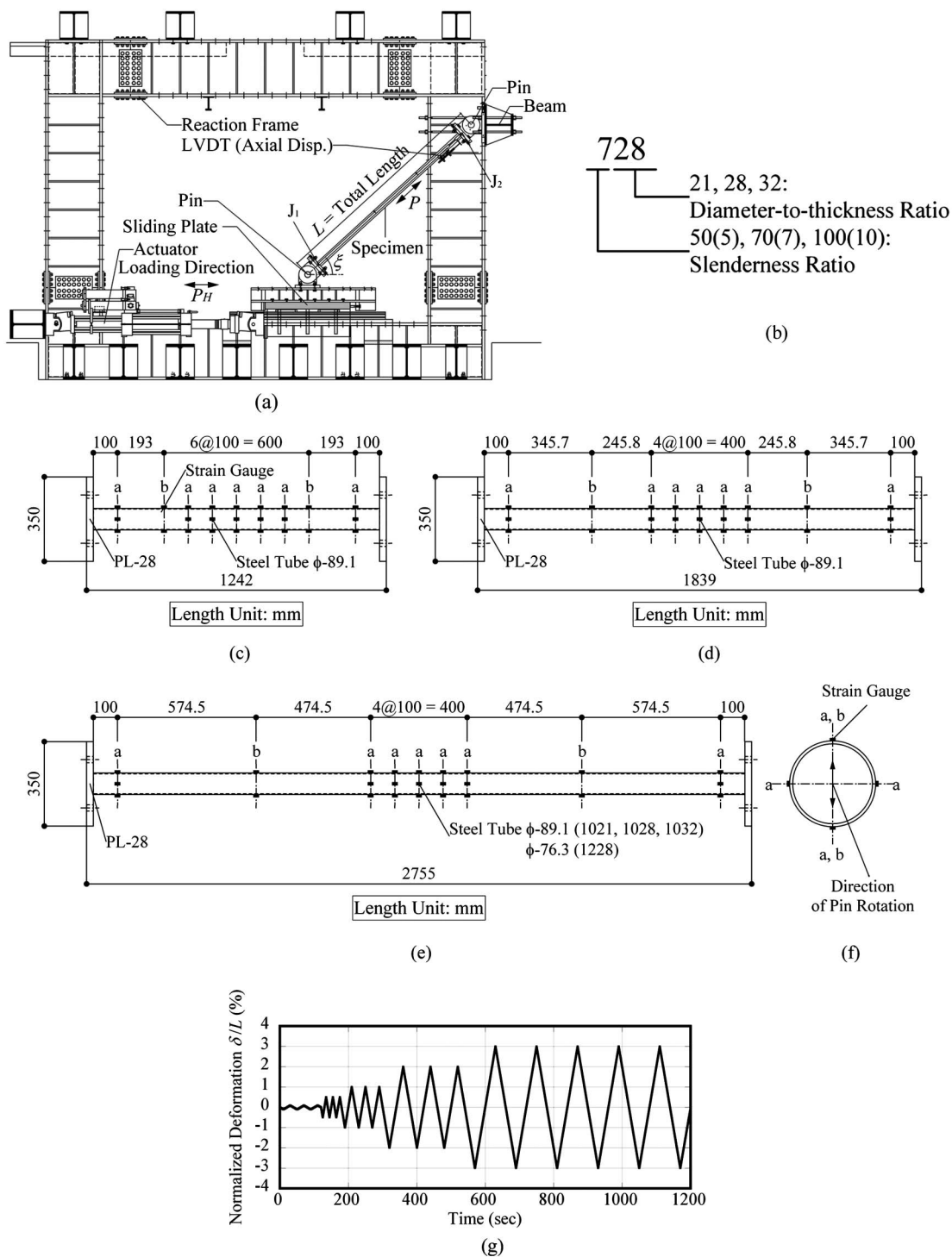


Fig. 1. Specimens and setup for cyclic loading tests on circular tube braces: (a) setup; (b) specimen designation; (c) Specimens 521, 528, and 532; (d) Specimens 721, 728, and 732; (e) Specimens 1021, 1028, 1032, and 1228; (f) strain gauge position; (g) test normalized deformation protocol

$$\epsilon_n = \frac{\delta}{L}, \quad \sigma_n = \frac{P}{A} \quad (2)$$

where ξ denotes an angle between the horizontal line and the axis of the brace, as shown in Fig. 1(a); and A = original sectional area of the circular tube. These braces were subjected to increasing normalized deformations defined by Eq. (2) of 0.5%, 1.0%, 2.0%, and 3.0% (corresponding to story drift angle approximately 0.3% to 2.0%) until they fractured.

Specimen parameters are listed in Table 1 and the designation of specimens are shown in Fig. 1(b). These parameters

comprised four slenderness ratios of approximately $\lambda = 50, 70, 100,$ and $120,$ and three diameter-to-thickness ratios $D/t = 21, 28,$ and $32.$ Figs. 1(c)–1(f) show the shapes of the specimens, and Table 2 lists the mechanical properties of the STK400 steel (JIS G 3444) used.

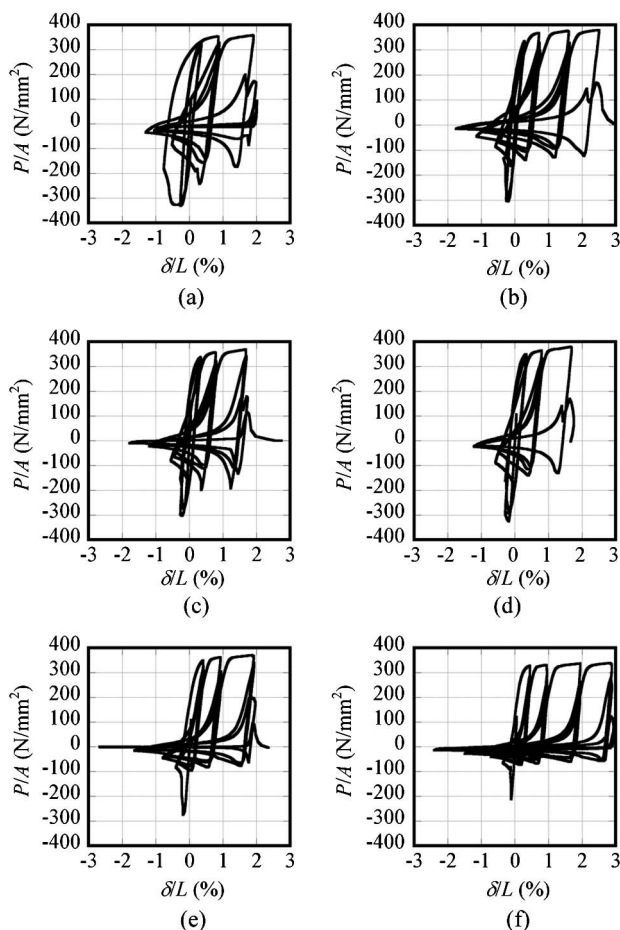
The surface strains in the specimens were detected by strain gauges shown in Figs. 1(c)–1(f). Fig. 1(g) exhibits the given test normalized axial deformation protocol. Fig. 2 shows the normalized force-deformation hysteresis curves obtained in the tests. Table 3 lists the results of the tests, including those of test

Table 1. Specimen Parameters

Specimen	Diameter D (mm)	Thickness t (mm)	Total length L (mm)	Diameter- to-thickness ratio D/t	Slenderness ratio λ
528	89.1	3.2	1,622	28	53
532		2.8	1,622	32	53
721		4.2	2,219	21	74
728		3.2	2,219	28	73
732		2.8	2,219	32	73
1021		4.2	3,135	21	104
1028		3.2	3,135	28	103
1032		2.8	3,135	32	103
1228	76.3	2.8	3,135	27	121

Table 2. Mechanical Properties of Steel

Specimen	Material	Equivalent yield stress σ_y (N/mm ²)	Equivalent tensile strength σ_u (N/mm ²)	Fracture elongation E_{long} (%)
$\phi 76.3 \times 2.8$	JIS G3444	352.8	424.2	33.0
$\phi 89.1 \times 2.8$	STK400	356.6	405.5	23.0
$\phi 89.1 \times 3.2$		348.9	415.9	30.2
$\phi 89.1 \times 4.2$		366.1	413.8	30.7

**Fig. 2.** Hysteresis curves obtained for different specimens in cyclic loading tests: (a) Specimen 528; (b) Specimen 721; (c) Specimen 728; (d) Specimen 732; (e) Specimen 1028; (f) Specimen 1228

cycles in which overall buckling, local buckling at the midpoint of the specimens, crack formation in the local buckling zone, and ultimate fracture occurred. All specimens exhibit overall buckling when normalized axial deformation was in a range of 0.3–0.8% and local buckling in a range of 0.6–2.0%. Subsequent to the occurrence of local buckling, all specimens are fractured at normalized deformation in the range of 1.0–2.6%. Fig. 3 depicts a tube surface strain transition by strain gauge in the local buckling zone; the tube surface strain increases drastically after local buckling occurs. Figs. 4(a) and 4(b) show the local buckling progression and the fractured section for Specimen 732, respectively. This image shows how the midpoint section of the circular tube deforms toward an eventual V-shape. Fig. 5 shows plots of the cumulative normalized deformation $\sum \Delta \varepsilon_n$ until fracture versus D/t [Fig. 5(a)] and λ [Fig. 5(b)]. In both instances, cumulative normalized deformation demonstrates a clear relationship to λ and D/t , increasing as λ increases or D/t decreases.

Analysis of Cyclic Loading Tests on Circular Tube Braces by FEM Analysis

The behavior of the circular tube braces after local buckling obtained from the experiment was studied through FEM analysis using ABAQUS Version 6.7-1. Fig. 6 shows the analysis model construction. End connections were assumed to be rigid, and half of the specimen length was modeled by symmetric boundary condition. The circular tube is composed of shell elements. Each element contained four nodes and three shell layers with seven integration points in the direction of thickness. A constitutive model for the steel material characteristics was calibrated using the results of tension coupon tests, as shown in Fig. 6(c). Overall hardening involved isotropic and kinematic hardening, as shown in Eqs. (3) and (4):

$$\sigma_{ys} = \sigma_{|ys} + \sigma_{pl} \quad (3)$$

$$\sigma_{pl} = \frac{C_1}{C_2} (1 - e^{-C_2 \varepsilon_{pl}}) \quad (4)$$

where σ_{ys} = yield surface stress during isotropic hardening; $\sigma_{|ys}$ = yield surface stress at zero plastic strain; and σ_{pl} = plastic stress of the steel material after yielding; C_1 and C_2 = material parameters calibrated by tension coupon tests; and ε_{pl} = plastic strain. Here, Eq. (3) defines the yield surface of the steel material, and Eq. (4) defines the inelastic response of the material postyield. Fig. 7 shows that the normalized force-deformation hysteresis curves obtained by analysis are consistent with the experimental results. Fig. 8 shows the strain contours in the overall and local buckling phases in Specimen 728. Strain concentrations in the local buckling zone C become more significant in Fig. 8(b) than the overall buckling phase depicted in Fig. 8(a). Fig. 9 shows strain calculated from FEM transition at Point C; overall buckling was initiated at $\varepsilon_n = 0.3\%$, and local buckling can be observed in the second loading cycle at $\varepsilon_n = 0.6\%$, after which the calculated local strain increased significantly up to 20–30%.

Thus, the strain concentration at Point C after local buckling leads to brace fracture. The assessed cumulative plastic strain at this point until the instant of fracture observed in the experiments was compared with a fatigue curve calibrated from cyclic loading coupon tests of the steel material, as given in Eq. (5) (Saeki et al. 1995a, b):

$$\overline{\Delta \varepsilon_{hp}} = 35N_f^{-0.47} \quad (5)$$

Table 3. Results of Cyclic Loading Tests

Specimen	Overall buckling			Local buckling			Crack			Fracture		
	ϵ_n Input (%)	ϵ_n Output (%)	Cycle	ϵ_n Input (%)	ϵ_n Output (%)	Cycle	ϵ_n Input (%)	ϵ_n Output (%)	Cycle	ϵ_n Input (%)	ϵ_n Output (%)	Cycle
528	1	0.5	1	1	1.3	3	2	2	2	2	2	4
532	1	0.7	1	1	0.7	2	2	1.5	1	2	1.5	1
721	0.5	0.3	2	2	1.1	3	3	1.7	2	3	1.7	2
728	0.5	0.3	2	1	0.6	3	2	1.2	3	3	3	1
732	1	0.6	1	1	0.6	2	2	1.2	2	2	1.2	2
1021	0.5	0.4	1	2	1.5	3	3	2.5	2	3	2.5	2
1028	1	0.4	1	1	1.6	1	2	1.6	3	2	2.6	1
1032	0.5	0.4	1	1	0.7	3	2	1.6	2	2	1.6	2
1228	0.5	0.5	1	2	1.5	2	—	—	—	3	2.4	4

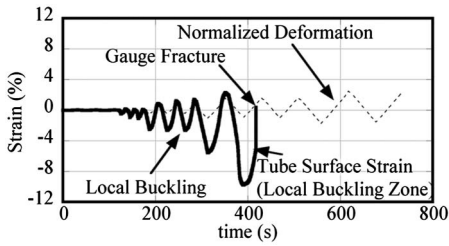


Fig. 3. Strain transition in local buckling zone



Fig. 4. Postbuckling behavior at the midpoint of specimens (Specimens 728 and 732): (a) local buckling ($\epsilon_n = 2.0\%$ first cycle); (b) fracture section (after $\epsilon_n = 2.0\%$ second cycle)

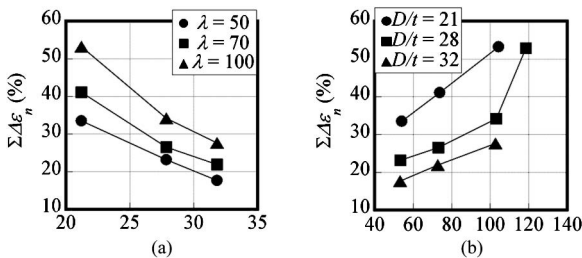


Fig. 5. Cumulative normalized deformation until fracture: (a) diameter-to-thickness ratio (D/t); (b) slenderness ratio (λ)

where $\overline{\Delta\epsilon_{hp}}$ = plastic local strain amplitude in the hinge zone; and N_f = number of cycles until steel fractures. This fatigue curve can be recalculated, taking into account the average of the plastic strain amplitude and the cumulative plastic strain, as shown in Eq. (6):

$$\Sigma\Delta\epsilon_{hp} = 2 \cdot N_f \cdot \overline{\Delta\epsilon_{hp}} = 3857 \overline{\Delta\epsilon_{hp}}^{-1.13} \quad (6)$$

Miner's rule is frequently used to evaluate the fatigue failure of steel subjected to a nonuniform cyclic loading history. In this study, the average amplitude of plastic strain is taken as a parameter.

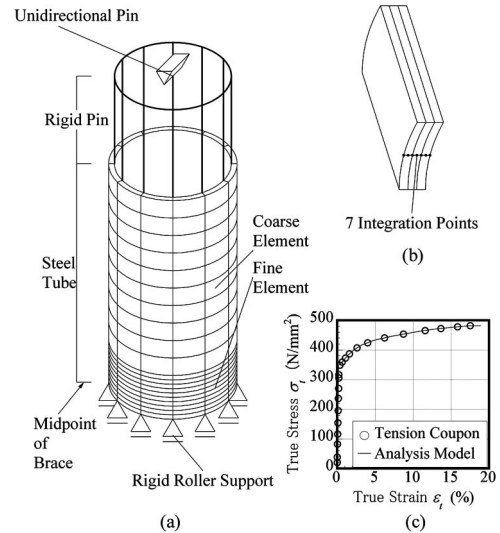


Fig. 6. FEM analysis model: (a) complete model; (b) shell section of steel tube; (c) material property (Specimen 728)

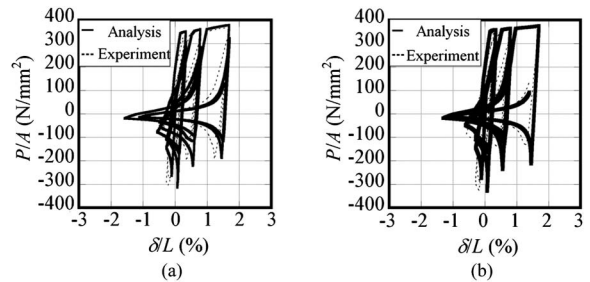


Fig. 7. Hysteresis curves obtained by analysis: (a) Specimen 728; (b) Specimen 732

The values estimated on such a basis agree with those obtained in applying Miner's rule when the exponent for N_f is close to -1.0 and exhibit no significant difference, even when shifted to approximately -0.5 . Fig. 10 shows the analytically obtained cumulative local plastic strain until the experimental instant of fracture versus the average plastic strain amplitude. These values generally agree with those obtained using the calibrated fatigue curve and applying local cumulative strain to the fatigue curve is considered valid for an approximate determination of the instant of fracture.

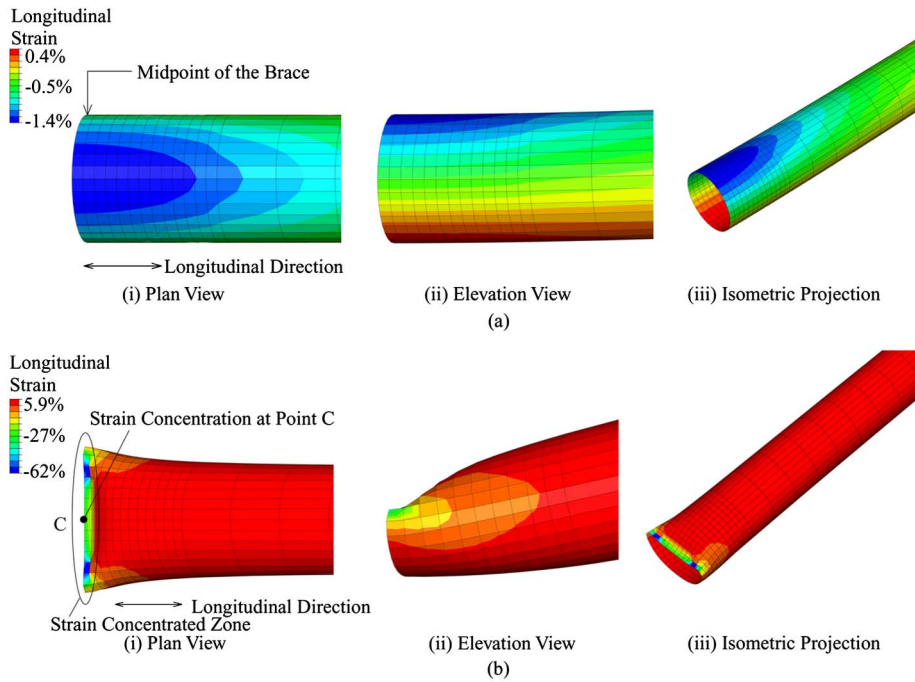


Fig. 8. Strain distribution obtained by analysis (Specimen 728): (a) overall buckling (equivalent strain 0.5%, first compression); (b) local buckling (equivalent strain 2.0%, second compression)

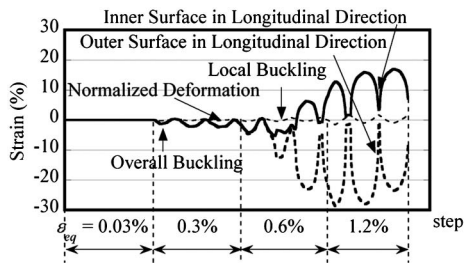


Fig. 9. Strain transition of steel tube surface (Specimen 728, Point C)

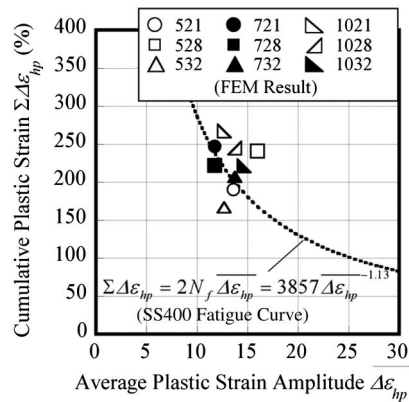


Fig. 10. Evaluation of cumulative plastic strain

Cumulative Deformation Capacity of Circular Tube Braces until Fracture

Subsequent to local buckling, the local strain in the buckling zone increases more drastically than that in other zones of the circular tube braces, which leads to fracture. Here, a practical model to predict the local strain transition and fracture in circular tube braces

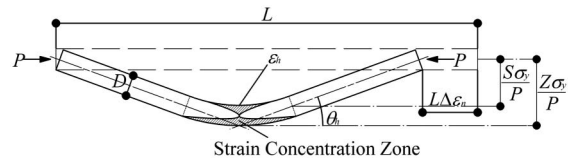


Fig. 11. Plastic hinge model for overall buckling

using the fatigue curve will be facilitated by postulating a simplified hinge zone model. During overall buckling, a plastic hinge is assumed to occupy the center of the circular tube brace, as shown in Fig. 11. The plastic zone length L_h is calculated using Eq. (7):

$$L_h = L \left[1 - \left(\frac{S}{Z} \right) \right] \quad (7)$$

where L = total length of circular brace defined previously; S = section modulus of circular tube; and Z = plastic section modulus of circular tube. The hinge angle θ_h is represented by Eq. (8), and the normalized deformation amplitude of braces $\Delta\epsilon_n$ on the compression side is assessed in Eq. (9), which includes a term for the maximum normalized tensile deformation, ϵ_{ntm} , observed before compression:

$$\theta_h = \cos^{-1}(1 - \Delta\epsilon_n) \quad (8)$$

$$\Delta\epsilon_n = \epsilon_{ntm} - \epsilon_n \quad (9)$$

The local strain in the hinge zone ϵ_h is calculated as an average approximation shown in Eq. (10):

$$\epsilon_h = \frac{\theta_h D}{L_h} = \frac{\theta_h D}{L \left[1 - \left(\frac{S}{Z} \right) \right]} = \frac{\theta_h D}{L \left(1 - \frac{\pi}{4} \right)} \quad (10)$$

where D = circular tube diameter. The circular tube deformation under conditions of local buckling is modeled as shown in Fig. 12. The relation in Eq. (11) defines the normalized deformation initiated by the local buckling ϵ_{lb} according to experimental data

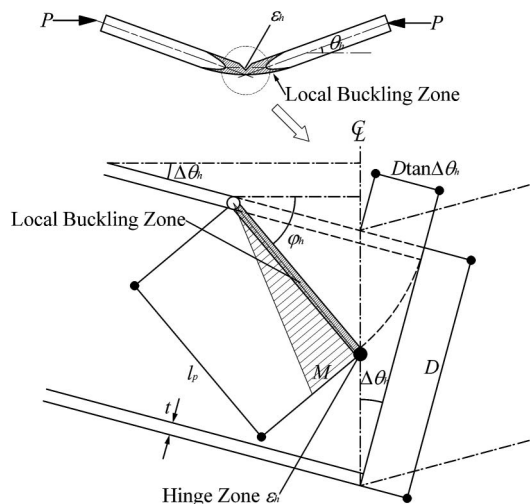


Fig. 12. Local buckling model for circular tubes

(Ogawa et al. 1995), and the hinge angle corresponding to local buckling may be calculated using Eq. (12), which is identical to Eq. (8):

$$\varepsilon_{lb} = 0.0683\varepsilon_y^{-0.39} \left(\frac{D}{t}\right)^{-1.39} \quad (11)$$

$$\theta_{lb} = \cos^{-1}(1 - \varepsilon_{lb}) \quad (12)$$

where ε_{lb} = normalized deformation attained at local buckling; ε_y = yield strain; t = circular tube thickness; and θ_{lb} = hinge angle attained at local buckling. The hinge angle increment at local buckling zone may be calculated using Eq. (13):

$$\Delta\theta_h = \theta_h - \theta_{lb} \quad (\theta_h > \theta_{lb}) \quad (13)$$

where $\Delta\theta_h$ = hinge angle increment that incites local buckling. The angle of the local buckling zone itself is calculated from Eq. (14) by using the hinge angle increment at which local buckling occurs, as shown in Fig. 12:

$$\varphi_h = \cos^{-1}\left(\cos \Delta\theta_h - \frac{D \sin \Delta\theta_h}{l_p}\right) \quad (14)$$

where φ_h = angle of skin plate at local buckling zone; and l_p = half-amplitude of local buckling wave, and all other variables have been defined previously. The half-amplitude of the local buckling wave is derived by way of classic theory using Eq. (15) (Timoshenko et al. 1961), where the plastic Poisson's ratio is $\nu_p = 0.5$:

$$l_p = \pi \sqrt[4]{\frac{D^2 t^2}{48(1 - \nu_p^2)}} = \pi \sqrt{\frac{Dt}{6}} \quad (15)$$

The strain in the hinge zone is taken to be the sum of overall and local buckling, as shown in Eq. (16):

$$\varepsilon_h = \frac{\varphi_h t}{2l_p(1 - \frac{S_l}{Z_l})} + \frac{\theta_{lb} D}{L(1 - \frac{S_l}{Z_l})} = \frac{3\sqrt{6}\varphi_h}{2\pi\sqrt{\frac{D}{t}}} + \frac{\theta_{lb} D}{L(1 - \frac{S_l}{Z_l})} \quad (16)$$

where S_l = section modulus of local buckling zone; Z_l = plastic section modulus of local buckling zone. Here, the local buckling zone is assumed as rectangular, and the ratio of section modulus (S_l/Z_l) is 2/3. Thus, the local strain is assessed at the local buckling zone both before and during overall buckling, in addition to throughout the local buckling process. Therefore, the strain concentration ratio α_c is defined by Eq. (17) as follows:

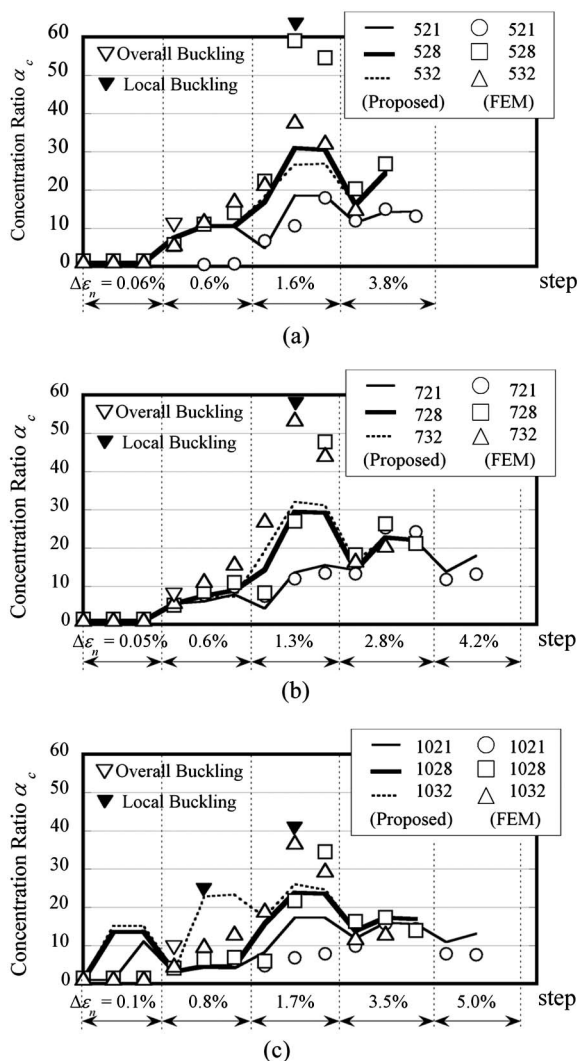


Fig. 13. Estimated strain concentration ratios: (a) Specimens 521, 528, and 532; (b) Specimens 721, 728, and 732; (c) Specimens 1021, 1028, and 1032

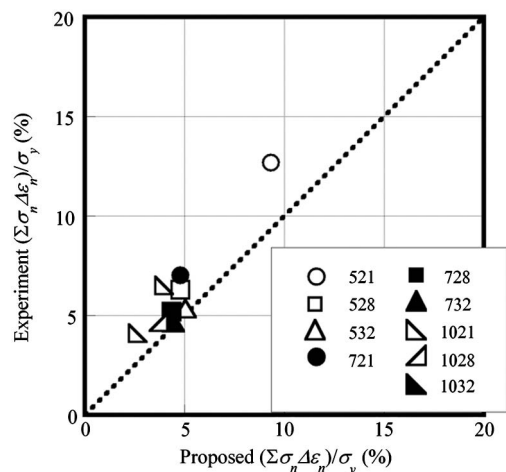


Fig. 14. Cumulative dissipated energy until fracture

$$\alpha_c = \frac{\varepsilon_h}{\varepsilon_n} = \begin{cases} 1.0 & (\Delta\varepsilon_n < \varepsilon_{cr}, \text{ Prebuckling stage and tensile stage}) \\ \frac{\theta_h D}{L(1 - \frac{\pi}{4})\varepsilon_n} & (\varepsilon_{cr} < \Delta\varepsilon_n < \varepsilon_{lb}, \text{ Overall buckling stage}) \\ \frac{3\sqrt{6}\varphi_h}{2\pi\sqrt{\frac{D}{t}}\varepsilon_n} + \frac{\theta_{lb} D}{L(1 - \frac{\pi}{4})\varepsilon_n} & (\varepsilon_{lb} < \Delta\varepsilon_n, \text{ Local buckling stage}) \end{cases} \quad (17)$$

where $\varepsilon_{cr} = \sigma_{cr}/E$ = normalized axial deformation corresponding to overall buckling; σ_{cr} = overall buckling stress; E = elastic modulus of steel, and all other variables have been defined previously. By employing Eq. (17), the local strain in the plastic hinge zone can be calculated from the total normalized deformation. The strain concentration ratios increase drastically after local buckling, and are larger for specimens with larger D/t and smaller λ , which generally agrees with the experimental results. The values calculated from Eq. (17) are plotted by the specified lines in Fig. 13 in accordance with the proposed method. They generally agree with those obtained by FEM analysis. Making use of this strain concentration ratio, the cumulative local strain transitions can be evaluated from ε_n protocol, and the instant of fracture can be evaluated by comparing cumulative local strain to the fatigue curves. In Fig. 14, cumulative dissipated energy as determined from the product of α_c and ε_n factored with fatigue criteria is compared with the experimental results. The estimates obtained by the proposed method are largely consistent with the experimental results, and this method is considered to be valid for fracture prediction.

Conclusion

The cumulative deformation capacity of tubular braces was investigated by performing cyclic loading tests for various slenderness and diameter-to-thickness ratios. The fracture mechanism is clarified by FEM analysis, the strain concentration ratio is defined by assuming a simple fracture model, and an easy prediction method for cumulative deformation capacity of circular tube braces under random cyclic loading is proposed. This study's conclusions may be summarized as follows:

1. Circular tube braces possessing 50–100 slenderness ratios and 20–30 diameter-to-thickness ratios are submitted to overall buckling at a normalized axial deformation of roughly 0.5%, local buckling at 1.0–2.0%, and fracture at 2.0–3.0%. Local buckling occurs earlier as the diameter-to-thickness ratio increases and the slenderness ratio decreases, and hence, the cumulative deformation capacity of the braces similarly decreases.
2. FEM results indicate that strain concentration increases significantly in the local buckling region, and the fracture point generally agrees with fatigue criteria based on averaged local plastic strain amplitude.
3. By using a simplified buckling model, the relationship between normalized deformation and local strain can be expressed by means of simple formulas within a defined strain concentration ratio index. Using such an index, a method is proposed to assess the cumulative deformation capacity of circular tube braces until fracture occurs. The results obtained by this proposed method agree overall with the experimental results, thereby satisfactory confirming their general validity.

Notation

The following symbols are used in this paper:

- A = original sectional area of circular tube;
- C_1, C_2 = material parameters for hardening rule calibrated by tension coupon tests;
- D = circular tube diameter;
- E = elastic modulus of steel;
- L = total length of circular brace;
- L_h = plastic hinge zone length;
- l_p = half-amplitude of local buckling wave;
- N_f = number of cycles until steel fractures;
- P = axial force of circular tube;
- S = section modulus of circular tube;
- S_l = section modulus of local buckling zone;
- t = circular tube thickness;
- Z = plastic section modulus of circular tube;
- Z_l = plastic section modulus of local buckling zone;
- α_c = strain concentration ratio;
- $\Delta\varepsilon_{hp}$ = plastic strain amplitude in hinge zone;
- $\overline{\Delta\varepsilon}_{hp}$ = average plastic strain amplitude in hinge zone;
- $\Delta\varepsilon_n$ = normalized axial deformation amplitude;
- $\Delta\theta_h$ = hinge angle increment that incites local buckling;
- δ = axial displacement of circular tube specimen;
- ε_{cr} = overall buckling normalized axial deformation (σ_{cr}/E);
- ε_h = strain in hinge zone;
- ε_{hp} = plastic strain in hinge zone;
- ε_{lb} = normalized deformation attained at local buckling;
- ε_n = normalized axial deformation;
- ε_{nfm} = maximum normalized tensile deformation;
- ε_{pl} = plastic strain;
- ε_y = yield strain;
- θ_h = hinge angle;
- θ_{lb} = hinge angle attained at local buckling;
- $\sum \Delta\varepsilon_{hp}$ = cumulative plastic strain in hinge zone;
- ν_p = plastic Poisson's ratio;
- σ_{cr} = overall buckling stress;
- σ_n = normalized stress;
- σ_{pl} = plastic stress of steel material after yielding;
- σ_{ys} = yield surface stress during isotropic hardening;
- $\sigma_{|ys}$ = yield surface stress at zero plastic strain; and
- φ_h = angle of skin plate at local buckling zone.

References

- ABAQUS Analysis Version 6.7-1 [Computer software]. ABAQUS, Inc. Pawtucket, RI.
- Elchalakani, M., Zhao, X.-L., and Grzebieta, R. (2003). "Tests on cold-formed circular tubular braces under cyclic axial loading." *J. Struct. Eng.*, 129(4), 507–514.
- Igarashi, S., Inoue, K., Kibayashi, M., and Asano, Y. (1972). "Hysteretic characteristics of steel-braced frames. Part 1: The behavior of bracing

- members under cyclic axial forces." *J. Struct. Constr. Eng., AIJ*, 196(6), 47–54 (in Japanese).
- Jain, A. K., Goel, S. C., and Hanson, R. D. (1978). "Inelastic response of restrained steel tubes." *J. Struct. Eng.*, 104(6), 897–910.
- Jain, A. K., Goel, S. C., and Hanson, R. D. (1980). "Hysteresis cycles of axially loaded steel members." *J. Struct. Eng.*, 106(8), 1777–1795.
- Kanvinde, A. M., and Deierlein, G. G. (2007). "Cyclic void growth model to assess ductile fracture initiation in structural steels due to ultra low cycle fatigue." *J. Eng. Mech.*, 133(6), 701–712.
- Nonaka, T. (1983). "Closed-form formulation for the hysteretic behavior of a bar under repeated axial loading—Part 1: Derivation of basic equations." *J. Struct. Constr. Eng., AIJ*, 334(12), 1–8 (in Japanese).
- Nonaka, T. (1984a). "Closed-form formulation for the hysteretic behavior of a bar under repeated axial loading -Part 2: Analytic Solution." *J. Struct. Constr. Eng., AIJ*, 338(4), 29–35 (in Japanese).
- Nonaka, T. (1984b). "Closed-form formulation for the hysteretic behavior of a bar under repeated axial loading. Part 3: Plastic straining and characteristic features." *J. Struct. Constr. Eng., AIJ*, 343(9), 42–49 (in Japanese).
- Ogawa, K., Kurobane, Y., and Maeda, T. (1995). "Post buckling behavior of circular tubular struts." *J. Struct. Constr. Eng., AIJ*, 475(9), 137–144 (in Japanese).
- Ookouchi, Y., et al. (2005). "Experimental studies of truss structures with hysteretic dampers." *Proc., Int. Symp. on Shell and Spatial Structures, IASS 2005*, Vol. 9, International Association for Shell and Spatial Structures, Madrid, Spain, 299–306.
- Popov, E. P., Zayas, V. A., and Mahin, S. A. (1979). "Cyclic inelastic buckling of thin tubular columns." *J. Struct. Eng.*, 105(11), 2261–2277.
- Prathuangsit, D., Goel, S. C., and Hanson, R. D. (1978). "Axial hysteresis behavior with end restraints." *J. Struct. Eng.*, 104(6), 883–896.
- Saeki, E., Sugisawa, M., Yamaguchi, T., Mochizuki, H., and Wada, A. (1995a). "A study on hysteresis and hysteresis energy characteristics of low yield strength steel." *J. Struct. Constr. Eng., AIJ*, 473(7), 159–168 (in Japanese).
- Saeki, E., Sugisawa, M., Yamaguchi, T., Mochizuki, H., and Wada, A. (1995b). "A study on low cycle fatigue characteristic of low yield strength steel." *J. Struct. Constr. Eng., AIJ*, 472(6), 139–147, (in Japanese).
- Shibata, M., Nakamura, T., and Wakabayashi, M. (1982). "Mathematical expression of hysteretic behavior of braces. Part 1: Derivation of hysteresis functions." *J. Struct. Constr. Eng., AIJ*, 316(6), 18–23 (in Japanese).
- Tang, X., and Goel, S. C. (1989). "Brace fractures and analysis of phase I structure." *J. Struct. Eng.*, 115(8), 1960–1976.
- Timoshenko, S. P., and Gere, J. M. (1961). *Theory of elastic stability*, 2nd Ed., McGraw-Hill, New York, 457–458.
- Tremblay, R. (2002). "Inelastic seismic response of steel bracing members." *J. Constr. Steel Res.*, 58(5-8), 665–701.